

## PERIDYNAMIC MODELING OF PLAIN AND REINFORCED CONCRETE STRUCTURES

**Walter Gerstle**

*Department of Civil Engineering  
University of New Mexico  
Albuquerque NM, 87131, USA  
Phone: (505) 277-3458, Fax: (505) 277-1988  
E-mail: gerstle@unm.edu*

**Nicolas Sau**

*Department of Civil Engineering,  
University of New Mexico,  
Albuquerque NM, 87131, USA  
Phone: (505) 277-3458, Fax: (505) 277-1988  
E-mail: nsau@unm.edu*

**Stewart Silling**

*Computational Physics Department, MS-0378  
Sandia National Laboratories  
Albuquerque, NM 87185-0378, USA  
Phone: (505) 844- 3973, Fax:(505) 844- 0918  
sasilli@sandia.gov*

### ABSTRACT

The peridynamic model was introduced by Silling in 1998. In this paper, we demonstrate the application of the quasistatic peridynamic model to two-dimensional, linear elastic, plane stress and plane strain problems, with special attention to the modeling of plain and reinforced concrete structures. We consider just one deviation from linearity - that which arises due to the irreversible sudden breaking of bonds between particles.

The peridynamic model starts with the assumption that Newton's second law holds true on every infinitesimally small free body (or particle) within the domain of analysis. A specified force density function, called the pairwise force function, (with units of force per unit volume per unit volume) between each pair of infinitesimally small particles is postulated to act if the particles are closer together than some finite distance, called the material horizon. The pairwise force function may be assumed to be a function of the relative position and the relative displacement between the two particles. In this paper, we assume that for two particles closer together than the specified "material horizon" the pairwise force function increases linearly with respect to the stretch, but at some specified stretch, the pairwise force function is irreversibly reduced to zero.

**Keywords:** Reinforced Concrete, Peridynamic, Damage, Fracture, Computational Mechanics

### 1. INTRODUCTION

The peridynamic model has been described in (Silling 1998; 2000; 2002; Silling, Zimmermann and Abeyaratne 2003; Silling and Askari 2003, Silling, Zimmermann and Abeyaratne 2003, Silling and Bobaru 2004, Gerstle and Sau 2004). In this paper, we demonstrate the application of the quasistatic peridynamic model to two-dimensional, linear elastic, plane stress and plane strain problems, with special attention to the modeling of plain and reinforced concrete structures. We consider a model for concrete with just one basic deviation from linearity - that which arises due to the irreversible sudden breaking of bonds between particles: a zeroth-order micro elastic damage model.

We limit our attention to zeroth-order micro elastic damage, quasistatic, rate-independent 2D modeling for three reasons. Firstly, we would like to demonstrate the behavior of the peridynamic model in its simplest nontrivial incarnations for clarity of presentation. Secondly, we demonstrate that 2D zeroth-order micro elastic quasistatic damage models represent an important class of behavior of concrete structures. Thirdly, our experience has shown that this class of models is the about as complex as can be successfully solved, given the computational limitations of contemporary single-processor computers.

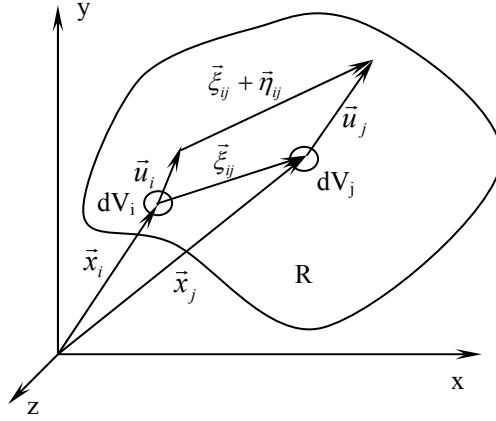


Figure 1. Terminology for peridynamic model.

The peridynamic model starts with the assumption that Newton's second law holds true on every infinitesimally small free body (or particle) within the domain of analysis. A specified internal force density function, called the pairwise force function, (with units of force per unit volume per unit volume) between each pair of infinitesimally small particles is postulated to act if the particles are closer together than some finite distance, called the material horizon. Within this material horizon, the pairwise force function may be assumed to be a function of the relative position and the relative displacement between the two particles. In the zeroth-order micro elastic damage model, we assume that for two particles closer together than the specified "material horizon" the pairwise force function increases linearly with respect to the stretch, but at some specified stretch, the pairwise force function is suddenly and irreversibly reduced to zero. Particles further apart than the material horizon do not interact with each other. (On the other hand, in the "first-order micro elastic damage model", not investigated further in this paper, the pairwise force function first increases linearly with respect to tensile stretch, and then beyond a particular stretch  $s_0$ , decreases linearly with increasing stretch, until at tensile stretch  $s_1$  and beyond, the pairwise force is zero.)

Refer to Figure 1 for terminology. We assume that Newton's second law holds true on an infinitesimally small particle  $i$ , with volume  $dV_i$ , mass  $dm_i$ , undeformed position  $\bar{x}_i$ , and displacement,  $\bar{u}_i$ , located within domain,  $R$ :

$$(dm_i)\ddot{\bar{u}}_i = \sum(d\bar{F}), \quad \text{Eq.1}$$

where  $\sum(d\bar{F})$  is the force vector acting on the free body, and in the quasistatic case,  $\ddot{\bar{u}}_i = 0$  is particle  $i$ 's acceleration. (The super-arrow signifies a vector quantity, while the over dot signifies differentiation with respect to time.)

Dividing both sides of Equation 1 by the differential volume of particle  $i$ ,  $dV_i$ , and partitioning the force into components internal and external to the system of particles under consideration gives

$$\rho\ddot{\bar{u}} = 0 = \bar{L} + \bar{b}, \quad \text{Eq.2}$$

where  $\rho$  is the mass density of particle  $i$  (at position  $\bar{x}_i$ ),  $\bar{L}$  is the force vector per unit volume due to interaction with all other particles (for example, particle  $j$ ) in domain  $R$ , and  $\bar{b}$  is the externally applied body force vector per unit volume.

The internal material force density per unit volume,  $\bar{L}$ , acting upon particle  $i$ , is an integral over all other particles,  $j$ , within the domain,  $R$ :

$$\bar{L} = \int_R (\bar{f}_{ij}) dV_j, \quad \text{Eq.3}$$

where  $\vec{f}_{ij}$  is the density of force densities between  $dV_i$  and the surrounding particles,  $dV_j$ . The pairwise force function,  $\vec{f}_{ij}$ , which has units of force per unit volume squared, can be viewed as a material constitutive property. In the simplest case, let us assume elastic behavior. In this case

$$\vec{f}_{ij} = \vec{f}_{ij}(\vec{u}_j - \vec{u}_i, \vec{x}_j - \vec{x}_i) = \vec{f}_{ij}(\vec{\eta}_{ij}, \vec{\xi}_{ij}), \quad \text{Eq.4}$$

so the pairwise force function is a function of relative displacement and relative position between particles i and j.

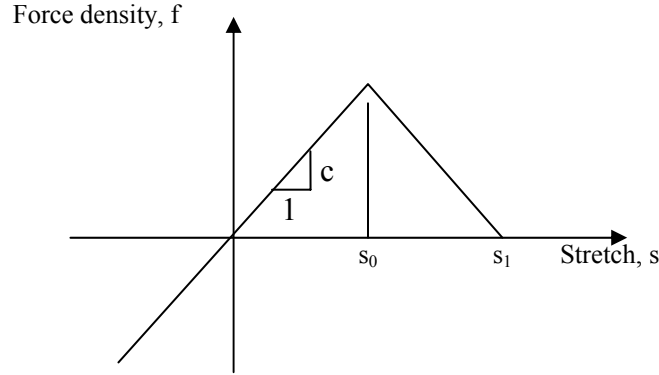


Figure 2. First order micro elastic peridynamic damage model.

This model governs the pairwise force density, of magnitude,  $f$ , between two particles situated within the material horizon,  $\delta$ , of each other. The zeroth order model results when  $s_0 = s_1$ ; the first order model results when  $s_0 < s_1$ .

Silling (Silling 1998) has proposed a simple nonlocal peridynamic constitutive model

$$\vec{f}_{ij}(\vec{\eta}_{ij}, \vec{\xi}_{ij}) = \frac{\mu \left( |\vec{\xi}_{ij} + \vec{\eta}_{ij}| - |\vec{\xi}_{ij}| \right) (\vec{\xi}_{ij} + \vec{\eta}_{ij})}{|\vec{\xi}_{ij} + \vec{\eta}_{ij}|} \quad \text{Eq.5}$$

if  $|\vec{\xi}_{ij} + \vec{\eta}_{ij}| - |\vec{\xi}_{ij}| < u^*$  and  $|\vec{\xi}_{ij} + \vec{\eta}_{ij}| < \delta$ , and  $\vec{f}_{ij}(\vec{\eta}_{ij}, \vec{\xi}_{ij}) = \vec{0}$  otherwise. Here  $\mu$ ,  $\delta$ , and  $u^*$  are positive “micro elastic” constants. Thus, the “spring” connecting any two particles is linear for small relative displacements, but it breaks when the relative displacement between the two particles exceeds  $u^*$ . Only particles within a distance  $\delta$  (the material horizon) from each other, in the undeformed configuration, interact. Equation (5) can be linearized as

$$f = \mu \left( |\vec{\xi} + \vec{\eta}| - |\vec{\xi}| \right), \quad \text{Eq.5a}$$

where it is understood that the pairwise force,  $f$ , is collinear with the undeformed positions of the two particles i and j, and  $f = 0$  if  $|\vec{\xi}| > \delta$ . In the case where the displacement due to deformation is small compared with the distance between the particles, the force magnitude is proportional, with microelastic constant  $\mu$ , to the change in *distance* between the two particles closer together than material horizon  $\delta$ , while the force is collinear with the undeformed positions of the two particles. (In the special case where  $|\vec{\xi}| = 0$ , the force is collinear with  $\vec{\eta}$ .)

In a slightly different version of the linearized pairwise force function (Silling and Askari 2003), the pairwise force function is assumed to be proportional to the stretch,  $s$ , rather than to the change in distance, between the two particles i and j. In this case,

$$f = c \left( \left| \vec{\xi} + \vec{\eta} \right| - \left| \vec{\xi} \right| \right) / \left( \left| \vec{\xi} \right| \right) = cs, \quad \text{Eq.5b}$$

where  $c$  is the microelastic constant relating force to stretch,  $s$ . In this version of the model, the bond irreversibly breaks when  $s > s_0$ , with  $s_0$  called the critical stretch for bond failure.

A first order micro elastic peridynamic damage model is shown in Figure 2. When  $s_0 = s_1$  this model results in the “zeroth order micro elastic damage” peridynamic model used in the remainder of this paper.

## 2. RELATIONSHIP BETWEEN MICROELASTIC AND CONVENTIONAL ELASTIC CONSTANTS

Let us consider first a linear elastic, isotropic, plane stress or plane strain structure, of thickness,  $t$ , with micro elastic constant  $c$  and material horizon,  $\delta$ . What are the corresponding Young’s modulus,  $E$ , and Poisson’s ratio,  $\nu$ ?

We require that the strain energy density,  $U_{E1}$ , due to a uniform principal strain state ( $s = \varepsilon_1 = \varepsilon_2$ ) be equal to the integral of the strain energy of the pairwise peridynamic forces,  $f$ , ( $U_{M1}$ ) arising from a kinematically equivalent displacement field, as shown in Fig. 3a. Also, the strain energy density,  $U_{E2}$ , due to a uniform shear strain ( $\varepsilon = \varepsilon_1 = -\varepsilon_2$ ) should be equal to the integral of the strain energy of the kinematically equivalent pairwise forces,  $f$ , ( $U_{M2}$ ) arising from a kinematically equivalent displacement field, as shown in Fig. 3b. Note that for an isotropic material (after rotation to principal directions) any other plane strain state can be considered as the linear superposition of these two strain states.

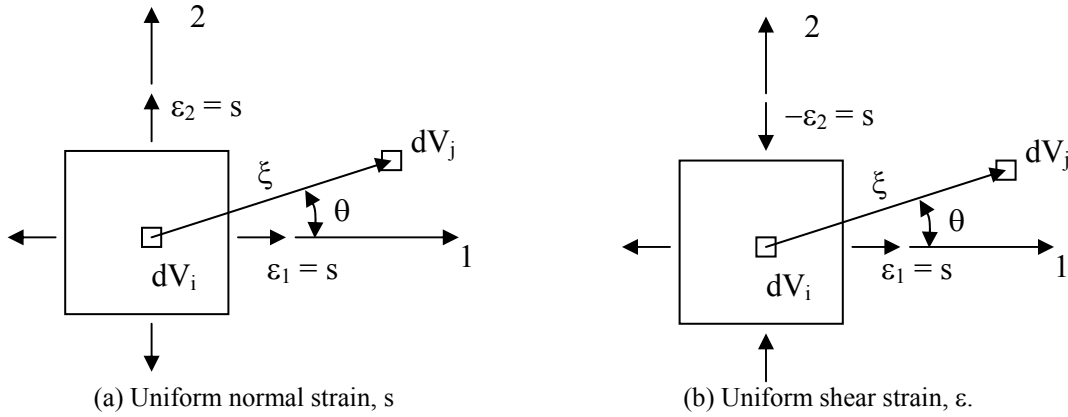


Fig. 3 – Figure used to derive relationship between microelastic and elastic constants.

It can be shown from conventional theory of linear elasticity, that  $U_{E1} = \frac{Es^2}{(1-\nu)}$  for plane stress and  $U_{E1} = \frac{Es^2}{(1+\nu)(1-2\nu)}$  for plane strain. Also, from the conventional theory of linear elasticity,  $U_{E2} = \frac{Es^2}{(1+\nu)}$  for a state of pure shear, shown in Fig. 3b, regardless of whether the problem is plane stress or plane strain.

On the other hand, from the two-dimensional peridynamic theory,  $U_{M1} = cs^2\pi\delta^3/6$  for the case of uniform normal stretch shown in Fig. 3a, and  $U_{M2} = cs^2\pi\delta^3/12$  for the case of pure shear shown in Fig. 3b. Solving the equations  $U_{E1} = U_{M1}$  and  $U_{E2} = U_{M2}$  simultaneously for  $E$  and  $\nu$ , we obtain

$$E = c\pi\delta^3(1+\nu)/12 \quad \text{Eq. 6}$$

with  $\nu = 1/3$  for plane stress and  $\nu = 1/4$  for plane strain.

A similar calculation for fully three-dimensional behavior shows that  $E = c\pi\delta^4/12$  and  $\nu = 1/4$ . In (Silling and Askari 2003), an implied formula  $E = c3\pi\delta^4/4$  appears to be in error. It is worthwhile to note that the plane stress Poisson’s ratio is different from the value of the 3D Poisson’s Ratio of  $1/4$  computed in (Silling 1998). It is apparent that by appropriately choosing peridynamic constants  $c$  and  $\delta$ , isotropic plane stress or plane strain

structures can be represented. However, the peridynamic model considered in this paper restricts Poisson's Ratio to  $\nu = 1/3$  for plane stress problems, and  $\nu = 1/4$  for plane strain problems.

It is important to understand that the peridynamic model predicts a more flexible, anisotropic material within a distance of the material horizon,  $\delta$ , of material boundaries. This is because particles closer than the material horizon to the boundary are connected to fewer other particles, have fewer pairwise forces, and thus have reduced stiffness. However, it is possible to maintain constant material stiffness close to domain boundaries through an appropriate discretization strategy involving a "ghost domain" with zero micro-elastic constant  $c$  surrounding the domain of interest.

### 3. NUMERICAL IMPLEMENTATION OF ELASTIC MODEL

We have written a 2D, linear elastic, static, plane stress and plane strain, program in MatLab, called Peri2D. Straight linear elastic reinforcing bars may be included. At the current time, only rectangular geometric regions have been implemented. The structure of the input file, shown in Fig. 4, and node patterns, shown in Fig. 5, indicate the scope of the peridynamic model. Figure 6 shows an example problem, a uniformly loaded cantilever reinforced concrete beam, together with the model definition for input to Peri2D. "Ghost nodes", discussed later, surround the beam.

**Model Definition for Peri2D**

**node\_pattern:** 'hexagonal' or 'rectangular' pattern of nodes, as shown in Fig. 5.

**num\_nodes\_horizontal:** the number of vertical columns of nodes, as shown in Fig. 5.

**material\_horizon:** radius of the material horizon, as shown in Fig. 5.

**problem\_type:** 'plane\_stress' or 'plane\_strain'

**regions** = [x<sub>min1</sub> x<sub>max1</sub> y<sub>min1</sub> y<sub>max1</sub>;  
x<sub>min2</sub> x<sub>max2</sub> y<sub>min2</sub> y<sub>max2</sub>;  
⋮  
x<sub>minN</sub> x<sub>maxN</sub> y<sub>minN</sub> y<sub>maxN</sub>] (each row defines a rectangular region)

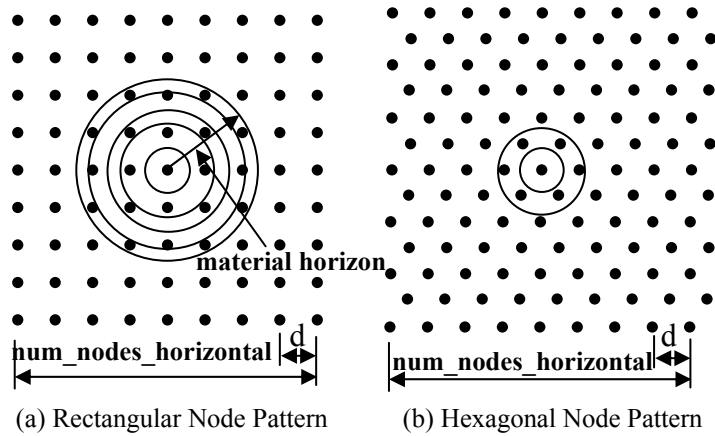
**mats** = [E<sub>1</sub> G<sub>f1</sub> region<sub>1</sub>;  
E<sub>2</sub> G<sub>f2</sub> region<sub>2</sub>;  
⋮  
E<sub>M</sub> G<sub>fM</sub> region<sub>M</sub>] (region<sub>i</sub> refers to row i defined in **regions**)

**bcs** = [code<sub>x1</sub> code<sub>y1</sub> value<sub>x1</sub> value<sub>y1</sub> region<sub>1</sub>;  
code<sub>x2</sub> code<sub>y2</sub> value<sub>x2</sub> value<sub>y2</sub> region<sub>2</sub>;  
⋮  
code<sub>xP</sub> code<sub>yP</sub> value<sub>xP</sub> value<sub>yP</sub> region<sub>P</sub>] (code: 0 = fixed; 1 = free) (value = body force or displacement)

**rebar** = [E<sub>1</sub> F<sub>y1</sub> A<sub>1</sub> x<sub>i1</sub> y<sub>i1</sub> x<sub>f1</sub> y<sub>f1</sub>;  
E<sub>2</sub> F<sub>y2</sub> A<sub>2</sub> x<sub>i2</sub> y<sub>i2</sub> x<sub>f2</sub> y<sub>f2</sub>;  
⋮  
E<sub>R</sub> F<sub>yR</sub> A<sub>R</sub> x<sub>iR</sub> y<sub>iR</sub> x<sub>fR</sub> y<sub>fR</sub>] (Young's Modulus, Yield Strength, Area, start and end positions)

Figure 4 – MatLab input file format for Peri2D.

The discretized peridynamic model is essentially a grid of nodes connected together with links (truss elements) of appropriate stiffness. Peri2D automatically computes the stiffness of each link by considering the strain energies,  $U_{E1}$  and  $U_{E2}$  of a single node,  $i$ , embedded within two homogeneous strain fields (uniform normal strain, and pure shear, as depicted in Fig. 3). For strain energy equivalence between the conventional theory of elasticity and the (discretized) peridynamic theory,  $U_{E1}$  and  $U_{E2}$  stored in the volume of node  $i$  should be equal to one-half of the strain energies,  $U_{M1}$  and  $U_{M2}$ , stored by all links connected to node  $i$ .



Material Horizon Level	Node Pattern = 'Rectangular'		Node Pattern = 'Hexagonal'	
	Number of nodes enclosed	Radius to most distant node /d	Number of nodes enclosed	Radius to most distant node /d
0	1	0	1	0
1	5	1	7	1
2	9	1.414	13	1.732
3	13	2	19	2
4	21	2.236	31	2.646
5	25	2.828	37	3
6	29	3	43	3.464
7	37	3.1623	55	3.606
8	45	3.606	61	4

Fig. 5 – Definition of node patterns and material horizon levels.

```

Example Model Definition for Peri2D:
Cantilever Reinforced Concrete Beam

num_nodes_horizontal = 14;
node_pattern = 'rec';
mat_horiz = 31.45;
problem_type = 'plane_stress';
regions = [-37.5 137.5 -87.5 287.5;
           0 100 0 200;
           0 100 -50 0;
           0 100 200 250];
mat_regions = [0.000001, 0.001, 1;
               3604, 0.001, 2;
               3604, 0.001, 3;
               3604, 0.001, 4];
bc_regions = [1 1 0 0 3;
              0 0 100 0 4];
rebar = [29000 60 1 12.5 -50 12.5 250];

```

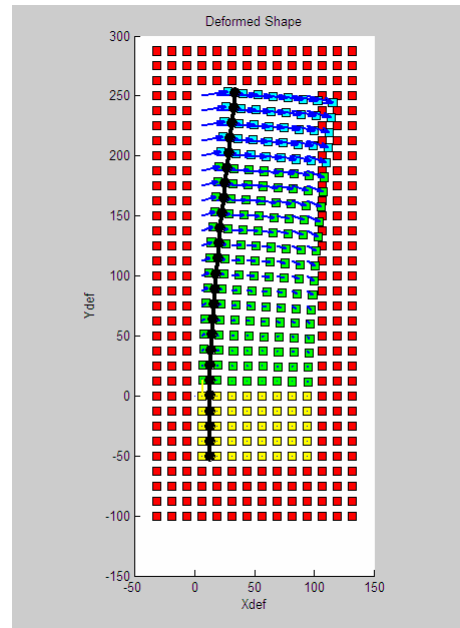


Fig. 6 – Example model for Peri2D: Cantilever Reinforced Concrete Beam, including “Ghost Nodes” Surrounding the Beam.

#### 4. CONVERGENCE STUDY OF ELASTIC BEHAVIOR

To demonstrate the elastic convergence behavior with model node refinement, we consider the bar with geometry shown in Fig. 7. The bar has modulus of elasticity  $E = 3604$  KSI and thickness,  $t = 1''$ . It is subject at its top and bottom ends to opposing uniformly distributed body forces  $B = 1$  Kip, applied in the  $y$  direction to simulate an axial load.

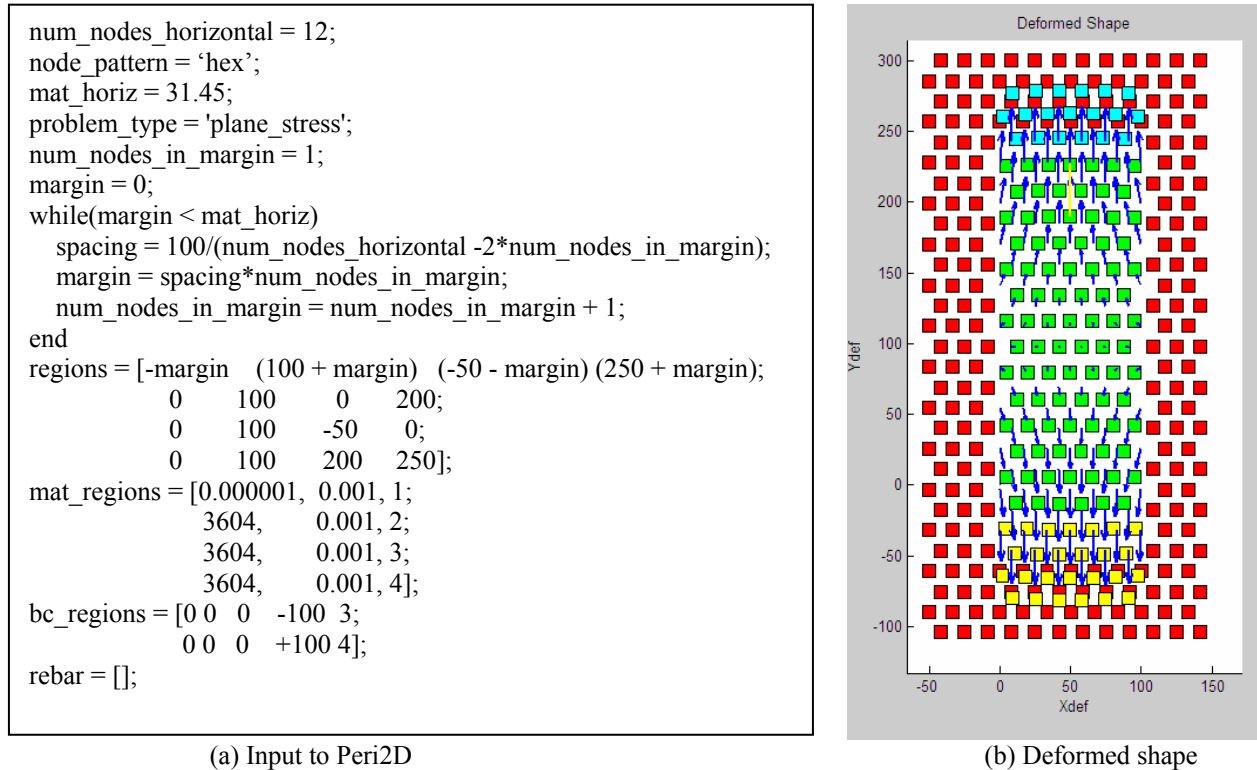


Fig. 7 – Problem for convergence study. (7 nodes spanning the specimen, hexagonal node pattern.)

A typical deformed shape from Peri2D is shown in Fig. 7b, and Table 1 provides convergence data – first for the rectangular node pattern, and then for the hexagonal node pattern. There are clearly some problems with uniform convergence. It is believed that these problems are related to (1) improper application of equivalent nodal loads, and (2) aliasing due to the fact that depending upon slight change in the specified number of nodes per row, an extra row or column of nodes may or may not be included within the geometric region of the domain. Both of these problems could be remedied relatively easily by using topological, rather than merely geometric definitions of the regions (Gerstle 2002). However, it is clear that for problems with reasonable numbers of nodes contained within a circle of radius equal to the material horizon,  $\delta$ , (say, 8 or greater), and reasonable numbers of nodes spanning each dimension (say, 12), the elastic displacements will be within 10 percent of the “exact” solution according to theory of continuum linear elasticity. There are some anomalies, perhaps due to a bug in Peri2D, particularly with the lateral strains with rectangular node patterns. The hexagonal node pattern appears to produce much better displacement predictions than the rectangular node pattern.

“Displacement Between Load Points” in Table 1 is computed as two times the total stored strain energy divided by the applied load at the top (and equal and opposite load applied at the bottom) of the specimen; it is thus a quantity that depends upon global results.

Although monotonic convergence characteristics with mesh refinement are not observed, the computed displacements are adequate for most practical structural engineering purposes. Perhaps future work will identify why better convergence characteristics were not obtained.

Table 1 – Results of Linear Elastic Convergence Study

Axial Bar – Rectangular Node Pattern – Convergence Study Results						
Number of nodes spanning specimen in the short (x) direction	Response Type					
	Percent error in Strain, $\epsilon_x$ at center of specimen (exact = 0.00009249)	Percent error in Strain, $\epsilon_y$ at center of specimen (exact = 0.00027747)	Percent error in Poisson's Ratio at center of specimen (exact = 0.3333)	Percent error in Displacement Between Load Points (exact = 0.06474 in.)	Number of Peridynamic Links per node	Node Spacing (inches)
4	-100.00	0.00	-100.00	-2.38	4	25
5	25.06	0.14	24.89	-1.56	8	20
6	25.27	0.15	25.08	-3.58	8	16.667
7	-41.76	0.67	-42.15	-0.67	12	14.286
8	-3.08	0.77	-3.83	-6.47	20	12.5
9	31.61	0.22	31.32	-4.40	24	11.111
10	-2.72	0.76	-3.45	-4.98	28	10
11	-12.87	0.72	-13.49	-3.25	36	9.0909
12	15.06	0.52	14.46	-5.70	44	8.3333
13	-3.67	0.68	-4.32	-3.23	48	7.6923
14	-3.13	0.70	-3.80	-5.96	60	7.1429
15	3.51	0.65	2.84	-5.41	68	6.6667
16	10.23	0.63	9.54	-6.28	80	6.25
17	-3.46	0.69	-4.12	-4.91	88	5.8824
18	4.51	0.61	3.87	-4.84	100	5.5556

Axial Bar – Hexagonal Node Pattern – Convergence Study Results						
Number of nodes spanning specimen in the short (x) direction	Response Type					
	Percent error in Strain, $\epsilon_x$ at center of specimen (exact = 0.00009249)	Percent error in Strain, $\epsilon_y$ at center of specimen (exact = 0.00027747)	Percent error in Poisson's Ratio at center of specimen (exact = 0.3333)	Percent error in Displacement Between Load Points (exact = 0.06474 in.)	Number of Peridynamic Links per node	Node Spacing (inches)
4	-9.30	-8.27	-1.12	-17.56	6	25
5	-4.87	-6.96	2.25	-18.12	6	20
6	-7.36	-7.01	-0.37	-7.95	12	16.667
7	-4.31	-5.64	1.41	-12.25	18	14.286
8	-3.87	-4.94	1.12	-11.22	18	12.5
9	-3.47	-4.59	1.17	-8.96	30	11.111
10	-2.72	-3.88	1.20	-9.95	36	10
11	-2.71	-3.56	0.89	-8.31	36	9.0909
12	-2.43	-3.34	0.94	-7.85	54	8.3333
13	-1.86	-2.87	1.04	-9.16	60	7.6923
14	-2.32	-2.88	0.57	-6.59	72	7.1429
15*	1.31	0.64	0.67	#VALUE!*	84	6.6667
16	-1.50	-2.25	0.77	-8.13	90	6.25
17*	1.10	0.56	0.53	#VALUE!*	108	5.8824
18	-1.30	-1.97	0.69	-8.51	120	5.5556

\* This discretization resulted in a large rigid body rotation, due to equal end moments caused by nodal antisymmetry at the two ends of the specimen.

## 5. NUMERICAL IMPLEMENTATION OF DAMAGE MODEL

We define the fracture energy,  $G_F$ , as the minimum energy required to separate a unit area of material. In the peridynamic model, the fracture energy can be calculated by integrating the breaking energy stored by all pairwise forces,  $f$ , crossing a unit area. The breaking energy per pairwise force between differential volume  $dV_i$  and differential volume  $dV_j$  is  $dU = (cs_0^2 \xi_{ij} / 2) dV_i dV_j$ , as shown in Fig. 2. Consider the one-dimensional peridynamic bar of cross-sectional area,  $A$ , shown in Fig. 8. The fracture energy is given by

$$G_F = \frac{1}{A} \int_{x_i=0}^{\delta} \left( \int_{\xi_{ij}=x_i}^{\delta} \left( \frac{cs_0^2 \xi_{ij}}{2} \right) (d\xi_{ij} A) \right) (dx_i A) = \frac{3Ac s_0^2 \delta^3}{2}, \text{ so}$$

$$s_0 = \sqrt{\frac{2G_F}{3Ac\delta^3}}. \quad \text{Eq. 7a}$$

Similar integrations yield

$$s_0 = \frac{2}{\delta^2} \sqrt{\frac{G_F}{ct}} \text{ in 2D, and} \quad \text{Eq. 7b}$$

$$s_0 = \sqrt{\frac{10G_F}{\pi c \delta^5}} \text{ in 3D.} \quad \text{Eq. 7c}$$

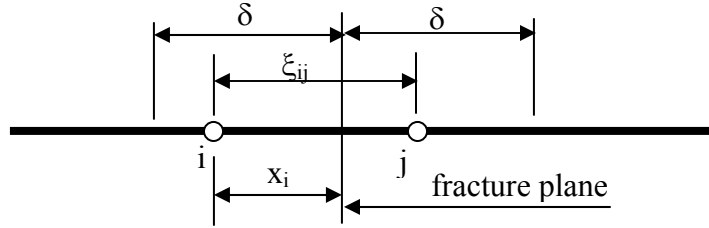


Fig. 8 – One-dimensional peridynamic bar, of cross-sectional area  $A$ .

The zeroth-order micro elastic damage model in Peri2D is simple: if the stretch between any pair of nodes exceeds  $s_0$ , the corresponding pairwise force  $f_{ij}$  is ignored in subsequent load steps. Thus, links between nodes are successively broken as they reach the micro elastic breaking stretch,  $s_0$ , and the load factor for each damage step is computed. So at each damage stage, the elastic response, as well as the load factor, is known.

The stiffness equations,  $[K]\{D\} = \{F\}$  are initially solved using efficient Cholesky factorization, implemented in MatLab using **chol(K)**. **chol(K)** uses only the diagonal and upper triangle of  $[K]$ , which is symmetric. If  $[K]$  is positive definite, then  $R = \mathbf{chol}(X)$  produces an upper triangular matrix,  $[R]$ , so that  $[R]^T[R] = [K]$ . Subsequently,  $\{Q\} = [R]^T\{F\}$  and  $\{D\} = [R]^{-1}\{Q\}$  are efficiently computed in turn.

Each damage stage involves a reduction in stiffness of the model. Rather than recreating the stiffness equations, it is much more efficient simply to update the already reduced stiffness matrix,  $[R]$ , using the MatLab function **cholupdate**, which produces a rank 1 update to the Cholesky factorization. If  $[R]$  is the original Cholesky factorization of  $[K]$ , then  $R1 = \mathbf{cholupdate}(R, X, '-')$  returns the upper triangular Cholesky factor of  $[K] - \{X\}\{X\}^T$ , where  $\{X\}$  is a column vector of appropriate length. **cholupdate** uses only the diagonal and upper triangle of  $[R]$ . As each bond is broken, its stiffness is computed and represented as  $\{X\}\{X\}^T$ , and the vector  $\{X\}$  is easily computed.  $R1 = \mathbf{cholupdate}(R, X, '-')$  returns the Cholesky factor of  $[K] - \{X\}\{X\}^T$ . Thus computations for each damage step are computationally efficient. For up to 5000 degrees of freedom, each Cholesky update is accomplished in a several seconds on a typical desktop computer. Thus, one hundred bonds may be broken in three or four minutes on a typical desktop computer. Larger problems bog down and become very slow because they cannot be solved in core memory. Much larger problems, with 50,000 or more degrees of freedom, could be solved on typical single processor desktop computers by using efficient out-of-core block solvers.

## 6. CALIBRATION OF MICROELASTIC DAMAGE MODEL

The zeroth order micro elastic damage model considered in this paper has three parameters: micro elastic constant,  $c$ , material horizon,  $\delta$ , and micro elastic breaking stretch,  $s_0$ . These three parameters may be adjusted to represent three of the most important characteristics of concrete: Young's modulus,  $E$ , uniaxial tensile strength,  $f'_t$ , and fracture energy,  $G_F$ .

Let us assume, heuristically, that the micro elastic breaking strain is equal to the uniaxial tensile strain:

$$s_0 = \varepsilon_t = \frac{f'_t}{E} \quad \text{Eq. 8.}$$

Combining Eqs. 6, 7b, and 8, we find that

$$\delta = \frac{4\pi EG_F}{9f_t'^2} \quad \text{Eq. 9}$$

Taking a typical concrete, with  $E = 3604$  ksi,  $f'_t = 0.4$  ksi, and  $G_F = 0.001$  k/in, we find that  $\delta = 31.45''$ . This implies that, to represent concrete, the node spacing in Peri2D should not exceed approximately  $\delta/3 = 10''$  if  $E$ ,  $f'_t$ , and  $G_F$  are to be faithfully reproduced. (However, the node spacing may be any value less than  $\delta/3$  for the purpose of analyzing small structures at high levels of spatial resolution.)

## 7. EXAMPLES OF DAMAGE IN PLAIN CONCRETE

Let us first consider a two-dimensional representation of a 100'' by 200'' long plain concrete block subject to first tension, then compression. We choose a typical concrete with  $E = 3604$  ksi,  $f'_t = 0.4$  ksi, and  $G_F = 0.001$  k/in, and thus, by Eq. 9,  $\delta = 31.45''$ . We analyze a 1'' thick slice of the 100'' by 200'' specimen, and assume plane stress conditions, as shown in Fig. 9.

The 50'' long end caps represented by regions 3 and 4 have the same Young's modulus as the central region 2, but the fracture energy,  $G_F$ , of the end caps is made very large to prevent damage at the ends of the specimen. Also, the fracture energy,  $G_F$ , of region 5, near the center of the specimen, is reduced by 5% to induce the initial tensile cracking to be reasonably centered in the specimen. (Rigid body displacements are suppressed by adding very small ( $10^{-10}$  k/in) stiffnesses along the main diagonal of the stiffness matrix. This way, if during the damage process a group of nodes becomes a completely detached rigid body, the incremental solution can continue. It is thus not necessary to supply specified displacement boundary conditions in the example problems considered here.)

In the nominal stress versus displacement plots of Figs. 10 and 11, the "nominal stress" is the load factor necessary to break the most highly stressed link, assuming an original applied load of 100 kips (on a specimen with cross-sectional area of 100 in<sup>2</sup>). The "displacement" is twice the current total strain energy divided by the current applied load. Results from Peri2D as well as approximate expected results (from the literature and the authors' experience, are shown as bold lines on the plots.

Figures 10, (a) (b) and (c) show the deformed grid at three different times during tensile loading, shown with exaggerated displacements. Readers may wonder why the result is asymmetric. Presumably this is because fracture, as a type of instability, introduces a source of randomness in the result.

On Figure 11(d), perhaps the under prediction of peak compressive stress at failure is due to the fact that the model only has a tensile failure mode in it, and bond strain at failure is assumed to be independent of what happens in other bonds. So, if we had a model in which bond strain at failure depends on local hydrostatic pressure, better agreement could be obtained. Indeed, subsequent calculations bear out this hypothesis.

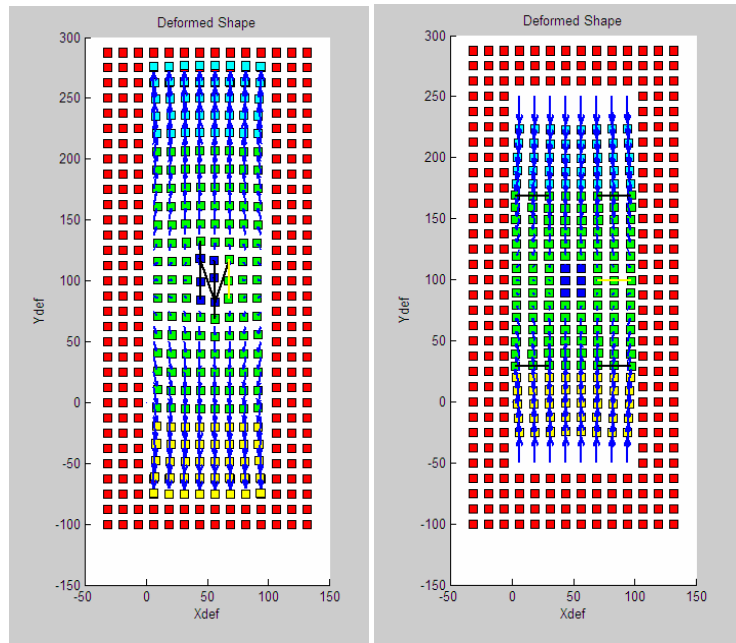
**Model Definition for Peri2D:**  
**Plain Concrete Cylinder in Tension**  
**(and in Compression)**

```

num_nodes_horizontal = 14;
node_pattern = 'rec';
mat_horiz = 31.45;
problem_type = 'plane_stress';
regions = [-37.5 137.5 -87.5 287.5;
           0 100 0 200;
           0 100 -50 0;
           0 100 200 250;
           35 65 85 115];
mat_regions = [0.000001, 0.001, 1;
              3604, 0.001, 2;
              3604, 1000., 3;
              3604, 1000., 4;
              3604, 0.00095, 5];
bc_regions = [0 0 0 (- or +)100 3;
              0 0 0 (+ or -)100 4];
rebar = [];

```

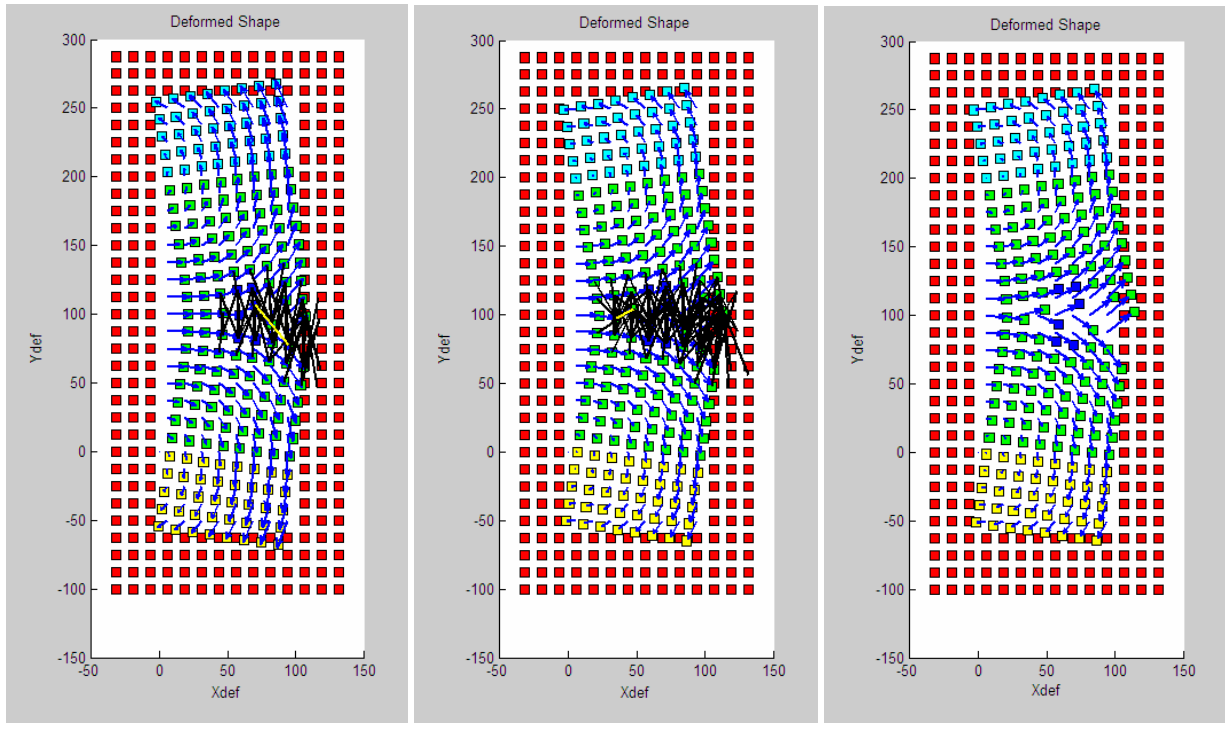
(a) Input data to Peri2D



(b) Tension

(c) Compression

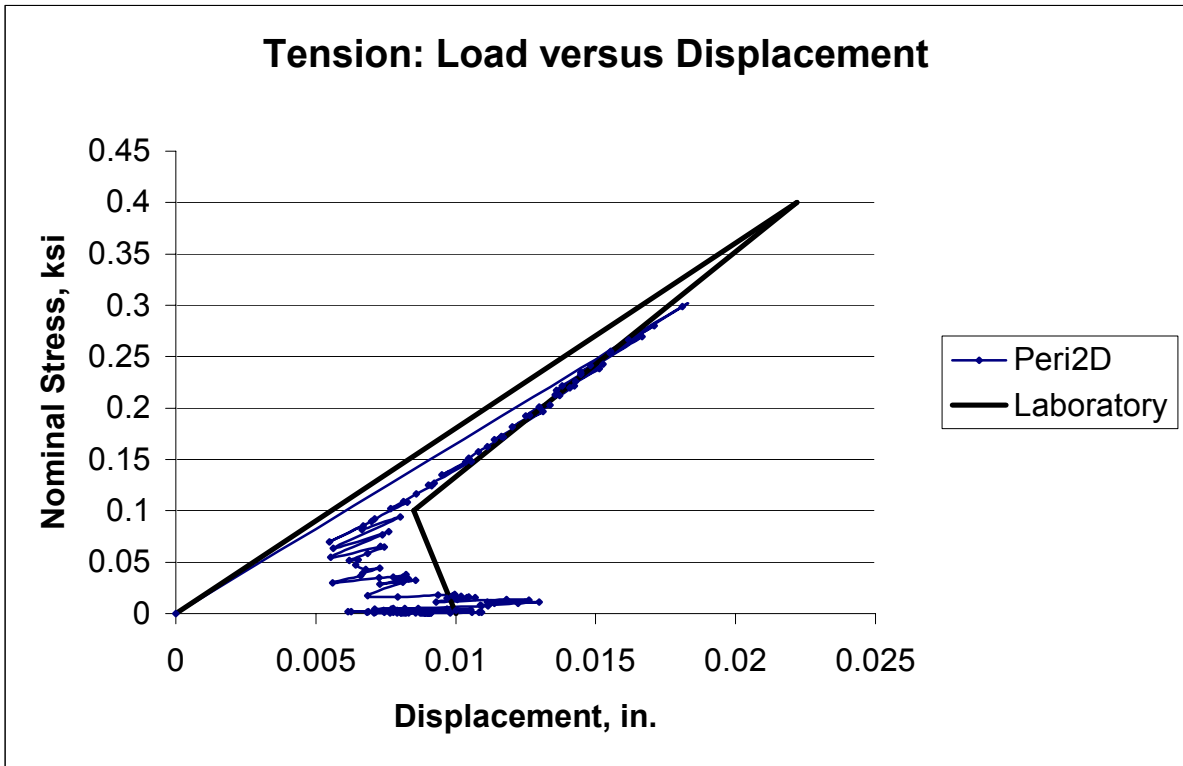
*Fig. 9 – Plane stress representation of concrete block in tension and in compression, showing broken bonds on magnified deformed shape after 10 damage steps.*



(a) 50 links broken

(b) 100 links broken

(c) 150 links broken



(d) Graph of Load Versus Displacement.

Fig. 10 – Deformed shape of the block in tension. Broken links are shown in (a) and (b).

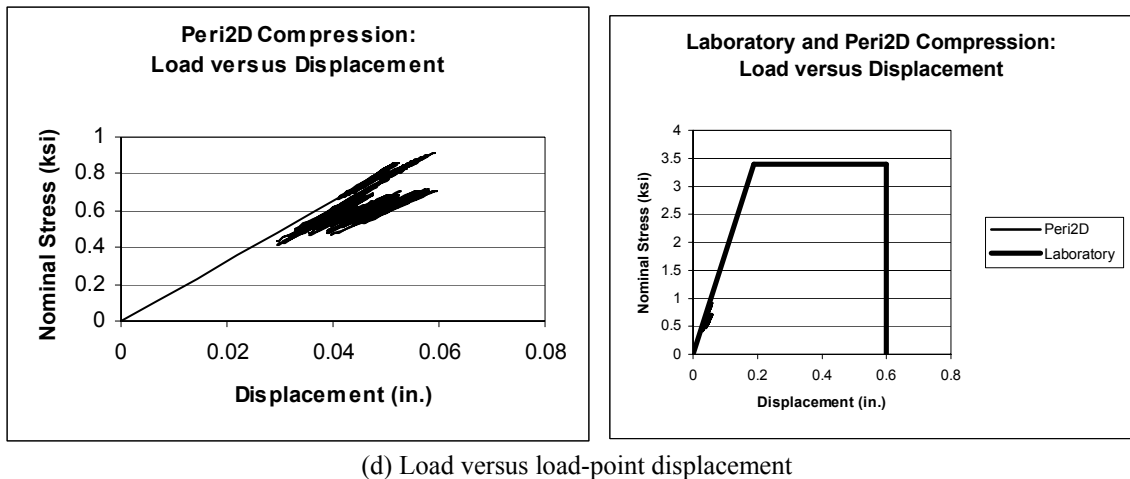
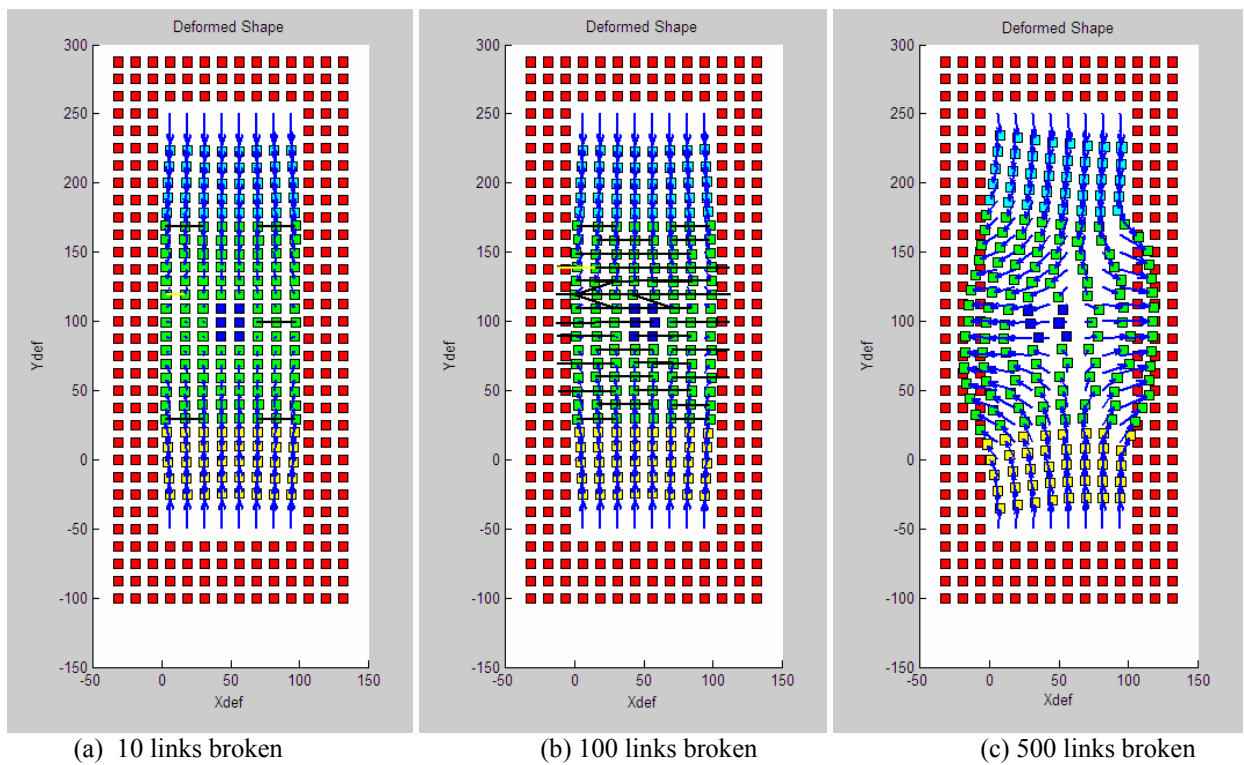


Fig. 11 – Deformed shape of the block in compression. Broken links are shown in (a) and (b).

## 8. REPRESENTATION OF REINFORCING BARS

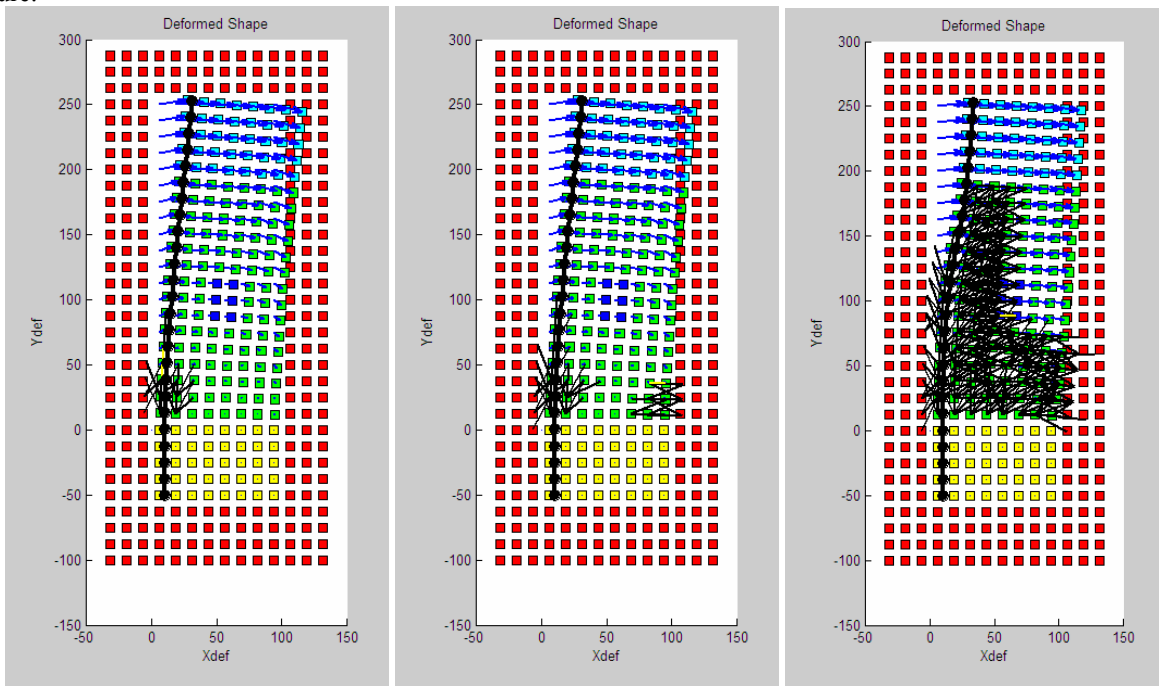
In Peri2D, reinforcing bars can currently be modeled as straight bars with linear elastic axial stiffness. (Elastoplastic behavior of the reinforcement could also be modeled, but the solution algorithm would be more complex and computationally expensive, so in this paper, plasticity of reinforcement is ignored. Thus, in this paper, only over-reinforced structures are considered.)

Although the reinforcing bars could be modeled using a one-dimensional peridynamic approach, because we know in advance that the bars will not fracture, we have chosen to model the reinforcing bars as simple continuum bar (truss) elements. The reinforcing bars are automatically divided into finite elements of equal length of approximately the node spacing of the peridynamic model. The nodes of the reinforcing bars are connected to the peridynamic concrete nodes using the micro elastic properties of the concrete nodes, on the assumption that the peridynamic nodes represent a weaker material. It would also be possible to provide a special peridynamic model to represent the behavior of the concrete/rebar interface (reflecting rebar rib behavior), but this has not been done here.

## 9. EXAMPLE OF DAMAGE IN REINFORCED CONCRETE

As an example of a reinforced concrete structure, we take the same specimen as that shown in Fig. 9, but add a single steel reinforcing bar (with Young's modulus  $E = 29,000$  ksi, yield strength  $f_y = 60$  ksi, and cross-sectional area  $A = 3$  in<sup>2</sup>) located 10" from the left side of the beam. The beam is over reinforced, and the steel will not yield. The boundary conditions are altered to represent a cantilever beam fixed at its base and loaded horizontally at its top end.

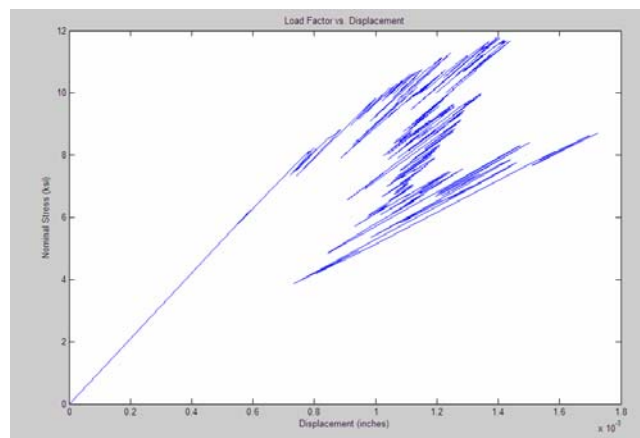
Note that in Fig. 12 (a) the breaking of links can be interpreted as cracking on the tension side of the beam, in Fig. 12 (b) the breaking of links on the compression side of the beam can be interpreted as a compression failure, and in Fig. 12 (c), in addition to extensive cracks on the tensile and compressive sides of the beam, there are bonds are broken through the mid-depth of the beam as well, in what we might interpret as diagonal shear cracking. Fig. 12(d) shows that stable crack growth is predicted initially as increasing load levels can be sustained, but that after a certain point, the cracks develop at ever decreasing loads, indicating what would in reality be a sudden, dynamic failure.



(a) 25 links broken

(b) 50 links broken

(c) 400 links broken



(d) Load versus load-point displacement

Fig. 12 – Magnified deformed shape of the singly reinforced cantilever beam.

## 10. CONCLUSIONS

The main conclusions that can be drawn from the present study, which considers a “peridynamic linear quasistatic zeroth-order micro elastic 2D damage model” are listed below.

- (1) The peridynamic model is capable of replicating the results of conventional linear elasticity by appropriately choosing the micro elastic constant,  $c$ , and the material horizon,  $\delta$ . However, the Poisson’s ratio is limited to  $1/3$  for plain stress, and  $1/4$  for plain strain problems. To eliminate strong boundary effects, it is necessary to include a “ghost domain” with null micro-elastic constant,  $c$ , surrounding, with margin at least equal to the material horizon, the domain of analysis.
- (2) Hexagonal and rectangular node patterns have been studied. The hexagonal pattern is superior because it provides improved material isotropy, more consistent Poisson’s ratio at coarse discretization, and more rapid convergence.
- (3) The convergence characteristics of the peridynamic model with discretization refinement is relatively poor in the current implementation. This is mostly due to biasing effects of nodes in relation to the specified geometry of the problem. This biasing problem could be avoided by modeling geometric domains as topological entities, each of which is discretized independently, as is further explained in [Gerstle 2002]. Also, application of proper work-equivalent nodal loads would help with convergence.
- (4) By appropriately choosing the micro elastic breaking strain,  $s_0$ , it is possible to objectively model the fracture energy,  $G_F$ , of an equivalent continuum.
- (5) The major elasticity and damage aspects of concrete behavior appear to be modeled correctly in a qualitative sense by the peridynamic model, even using the very basic (three parameter:  $c$ ,  $\delta$ ,  $s_0$ ) zeroth order peridynamic damage model described herein. However, the examples show that the quantitative agreement between the peridynamic model and the observed material behavior in the compressive regime is poor. Recent work has shown that a first order micro elastic damage model (with modification to account for enhanced micro elastic strength in the compressive strain regime) is promising for modeling concrete in compression.
- (6) One-dimensional models of discrete reinforcing bars can be easily added to two-dimensional plain concrete models, hence enabling the modeling of reinforced concrete structures.

## 11. REFERENCES

- Bazant, Z. P., and Jirasek, M., (Nov. 2002) “Nonlocal Integral Formulations of Plasticity and Damage: Survey of Progress”, *Journal of Engineering Mechanics*, Vol. 128, No. 11, pp. 119-1149.
- Gerstle, W., (2002), “Toward a Meta-Model for Computational Engineering”, *Engineering with Computers*, Vol. 18, Issue 4, pp 328-338, Springer-Verlag, London.
- Silling, S. A., (1998), “Reformation of Elasticity Theory for Discontinuous and Long-Range Forces”, SAND98-2176, Sandia National Laboratories, Albuquerque, NM.
- Silling, S. A., (2000), “Reformulation of Elasticity Theory for Discontinuities and Long-Range Forces”, *Journal of the Mechanics and Physics of Solids*, Vol. 48: pp. 175-209, Silling, S. A., “Dynamic Fracture Modeling With a Meshfree Peridynamic Code”, SAND2002-2959C, Sandia National Laboratories, Albuquerque, NM, 2002A.
- Silling, S. A., (2002), “EMU Website”, SAND2002-2103P, Sandia National Laboratories, Albuquerque, NM, 2002B.
- Silling, S. A., Zimmermann, M., and Abeyaratne, R., (2003), “Deformation of a Peridynamic Bar”, SAND2003-0757, Sandia National Laboratories, Albuquerque, NM.
- Silling, S. A. and Askari, E., (2003), “Peridynamic Modeling of Impact Damage”, unpublished to date.
- Silling, S. A. and Bobaru, F., (2004), “Peridynamic Modeling of Membranes and Fibers”, submitted to: *International Journal of Non-Linear Mechanics*.
- Gerstle, W. and Sau, N., (2004), “Peridynamic Modeling of Concrete Structures”, *Proceedings of the Fifth International Conference on Fracture Mechanics of Concrete Structures*, Li, Leung, Willam, and Billington, Eds., Ia-FRAMCOS, Vol. 2, pp. 949-956.